α-decay spectroscopy of the new isotope ^{192}At

A. N. Andreyev,[1] S. Antalic,[2] D. Ackermann,[3,8] S. Franchoo,[4] F. P. Heßberger,[3] S. Hofmann,[3,9] M. Huyse,[5] I. Kojouharov,[3] B. Kindler,[3] P. Kuusiniemi,[3] S. R. Lesher,[5] B. Lommel,[3] R. Mann,[3] G. Münzenberg,[3,8] K. Nishio,[3,10] R. D. Page,[6] J. J. Ressler,[7] B. Streicher,[2] S. Saro,[2] B. Sulignano,[3] P. Van Duppen,[5] and D. R. Wiseman[6]

[1]*TRIUMF, 4004 Wesbrook Mall, Vancouver, British Columbia, Canada, V6T 2A3*

[2]*Department of Nuclear Physics and Biophysics, Comenius University, Bratislava, SK-84248, Slovakia*

[3]*Gesellschaft für Schwerionenforschung, Planckstraße 1, D-64291 Darmstadt, Germany*

[4]*IPN Orsay, F-91406 Orsay Cedex France*

[5]*Instituut voor Kern- en Stralingsfysica, University of Leuven, B-3001 Leuven, Belgium*

[6]*Department of Physics, Oliver Lodge Laboratory, University of Liverpool, Liverpool L69 7ZE, United Kingdom*

[7]*Department of Chemistry, Simon Fraser University, Burnaby, British Columbia, Canada V5A-1S6*

[8]*Institut für Physik, Johannes Gutenberg-University, D-55099 Mainz, Germany*

[9]*Physikalisches Institut, J.W. Goethe-Universität, D-60054 Frankfurt, Germany*

[10]*Advanced Science Research Center, Japan Atomic Energy Agency, Tokai, Ibaraki 319-1195, Japan*

(Received 25 October 2005; published 28 February 2006)

Decay properties of the new neutron-deficient nuclide ^{192}At have been studied in the complete fusion reaction ^{144}Sm(^{51}V,3n)^{192}At at the velocity filter SHIP. Two isomeric states with half-lives of 88(6) ms and 11.5(6) ms, respectively, and with complex α-decay schemes were identified in ^{192}At. The decay pattern of one of the isomers suggests that it is based on the oblate-deformed $\pi 2f_{7/2} \otimes \nu 1i_{13/2}$ configuration, which confirms the expected onset of deformation in the At isotopes by approaching the neutron midshell at $N = 104$.

DOI: 10.1103/PhysRevC.73.024317 PACS number(s): 23.60.+e, 27.80.+w, 25.70.Hi

I. INTRODUCTION

Theoretical calculations have suggested shape coexistence and the onset of strong ground-state deformation in the extended region of nuclei just above the proton shell closure at $Z = 82$ and close to the neutron midshell at $N = 104$, see for example Ref. [1]. Unfortunately, due to large neutron deficit and strong fission competition the nuclei in this region are difficult to study experimentally. Only recently has detailed information on the deformed shapes in Bi and Po nuclei in this region started to emerge, both from in-beam and particle decay studies, see examples in Refs. [2–6] and extensive references therein.

In contrast to this, there exist only scarce data on shape coexistence in the very neutron-deficient At isotopes which is partly explained by their even higher fissility. Presently available in-beam techniques allow reliable studies of nuclei with production cross sections down to only a few hundred nanobarns, thus the most neutron-deficient At isotopes studied by this method are ^{196,197,199}At [7–10]. Further progress with in-beam studies is very difficult, both due to the relatively low beam intensities of $\sim$10 pnA used in such experiments (limited by the counting rate in a single Ge detector) and due to the relatively low γ-ray efficiency of the presently used in-beam techniques.

On the other hand, α decay is a powerful complementary tool to investigate low-energy shape coexistence and structure of the most neutron-deficient nuclei. The idea of the method is to study α decays of the parent isotope to the ground state and to low-lying excited states in the daughter nucleus. By comparing the strengths of these decays, expressed via the reduced α widths δ_α^2 [11], conclusions can be drawn on the structure and configuration of the states connected by the decay. One of the advantages of this method is that much higher beam intensities up to a few pμA can be used. Combined with efficient recoil separators and modern detection systems which are used at the focal plane, this allows detailed spectroscopic studies at a cross section level down to a few hundred picobarns. Relevant examples in the region of our interest are the recent α and α-γ study of ^{195}At [12] and identification of the new α emitters ^{191}At and ^{193}At [13], produced at the RITU gas-filled separator [14] with cross sections of about 300 pb and 40 nb, respectively.

It is well known that the ground state of the odd-mass At isotopes with $A \geqslant 197$ has spin-parity $I^\pi = 9/2^-$ and is interpreted as a nearly spherical $\pi 1h_{9/2}^3$ configuration. One of the important conclusions of Refs. [12,13] was that the $1/2^+$ state, which is understood as the intruder $\pi 3s_{1/2}^{-1} \otimes \pi 1h_{9/2}^4$ configuration in the spherical shell model, becomes the ground state in ^{191,193,195}At, with no evidence for the spherical $9/2^-$ state observed so far in these nuclei. In the deformed mean field approach this configuration corresponds to the occupation of the $1/2^+[440]3s_{1/2}$ Nilsson orbital. The occurrence of a deformed ground state in the light At isotopes is in an agreement with theoretical calculations [1], although the change of configuration was predicted to happen already between ^{198}At and ^{199}At. Furthermore, in contrast to the heavier At isotopes, the oblate-deformed $7/2^-[514]$ Nilsson state, originating from the $\pi 1h_{9/2}$ shell at sphericity and having mixed $\pi 1h_{9/2}/\pi 2f_{7/2}$ character at sufficiently large oblate deformation, becomes the first excited state situated slightly above the $1/2^+$ ground state in ^{191,193,195}At.

The study of odd-odd isotopes can shed extra light on the shape coexistence phenomena. However, such investigations are notoriously difficult due to the occurrence of proton-neutron (p-n) multiplets, which often result in isomeric states

and in a complex decay path of the isotopes of interest [15,16]. As a recent example of such work we refer to our detailed α-decay studies of the odd-odd ^{184,186,188,190}Bi isotopes [17,18], for which complex decay schemes involving p-n multiplet states were discussed.

In this work we report on the identification of isomeric states in the new isotope ^{192}At and on their detailed α and α-γ spectroscopy. It is necessary to note that in study [13], dealing with the identification of ^{191,193}At, a brief comment on the identification of ^{192}At was made, but no data on the half-life, α decay energy or decay scheme were given.

II. EXPERIMENTAL SETUP

The nucleus ^{192}At was produced by evaporation of three neutrons in the complete fusion reaction of ^{51}V ions with a ^{144}Sm target. A pulsed ^{51}V beam (5 ms on/15 ms off) with a typical intensity of about 150–200 pnA on target was provided by the UNILAC heavy ion accelerator of the GSI (Darmstadt, Germany). Eight 400 μg/cm^2 thick ^{144}Sm targets were mounted on a target wheel, rotating synchronously with the UNILAC macropulsing. The targets were produced by evaporating ^{144}SmF$_3$ material (96.47% isotopic enrichment) onto a carbon backing of 40 μg/cm^2 thickness and covered with a 10 μg/cm^2 carbon layer to increase the radiative cooling and reduce the sputtering of the material. A beam energy of $E(^{51}\text{V}) = 230(1)$ MeV in the middle of the target was used, which corresponds to the maximum of the excitation function for this nuclide calculated with the statistical model code HIVAP [19].

After separation by the velocity filter SHIP [20] the evaporation residues (EVRs) were implanted into a 300 μm thick, 35×80 mm^2 16-strip position-sensitive silicon detector (PSSD), where their subsequent particle decays were measured [21]. The α-energy calibration of the PSSD was performed by using $E_\alpha = 7167(4)$ decay of ^{192}Po [5] ($p2n$ channel of the studied reaction, Fig. 1(a) and the α lines at 5863(2) keV (^{200}Po), 6412(2) keV (^{200}At) and 6643(3) keV (^{199}At) [22]. The three latter nuclides were abundantly produced in reactions with the admixtures of heavier Sm isotopes in the target. In this experiment eight strips of the PSSD had an energy resolution of ~25 keV (FWHM) for the α line of ^{192}Po, while for the remaining 8 strips the energy resolution was in the range of 45–75 keV. For most of the data analysis this did not cause any problems and we used the data from all 16 strips; for example, the energy resolution of the ^{192}Po peak in Fig. 1(a) is 35 keV (FWHM). However, in a few cases when the good energy resolution could be important, representative spectra from the eight strips with the energy resolution of ~25 keV were also checked, see examples below.

Upstream of the PSSD, six silicon detectors having the same dimensions (called further "BOX detectors") were mounted in an open box geometry, see details in Ref. [23]. They were used to measure the energies of the particles (α, β and conversion electrons), escaping from the PSSD in the backward direction.

Three thin time-of-flight (TOF) detectors [24] were installed in front of the BOX+PSSD system allowing the reaction products to be distinguished from scattered beam

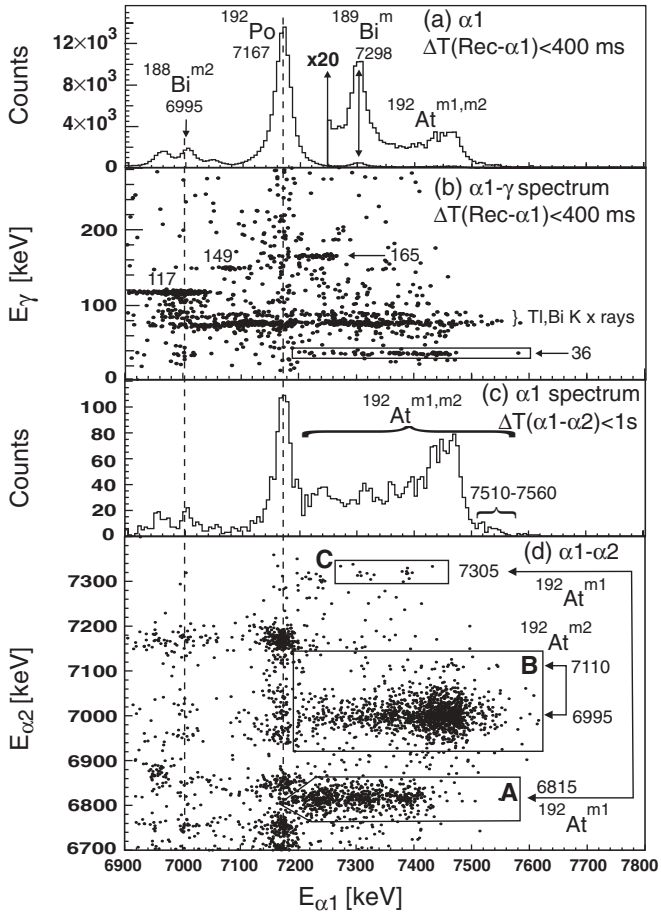

FIG. 1. (a) A part of the α1-energy spectrum from the reaction ^{51}V(230 MeV) + ^{144}Sm → ^{195}At* registered in the whole PSSD within 400 ms of a recoil implantation at the same PSSD location. Note the Y-scale change for $E_{\alpha 1} \geqslant 7250$ keV; α-decay energies are given in keV. (b) The $E_{\alpha 1}$-E_γ spectrum for α1 events in coincidence with γ rays, $\Delta T(\alpha 1\text{-}\gamma) \leqslant 5$ μs. Some γ-ray groups are indicated with their energies in keV. (c) The same as (a), but with a condition that the recoil-α1 pair must be followed by an α2 decay within the time interval of $\Delta T(\alpha 1\text{-}\alpha 2) \leqslant 1$ s. (d) The two-dimensional $E_{\alpha 1}$-$E_{\alpha 2}$ plot corresponding to (c). The energies of the daughter α decays of ^{188}Bi are shown in keV in panel (d).

particles. More importantly, decay events in the PSSD could be distinguished from the implantation events by requiring an anticoincidence condition between the signals from the PSSD and from at least one of the TOF detectors.

An additional 300 μm thick silicon detector similar in shape to the PSSD was installed 8 mm behind the PSSD. It was used to register the energy-loss signals of the high-energy protons and α particles produced in reactions on the carbon backing of the target and on the carbon charge equilibration foil installed a few cm downstream from the target. Such particles can pass through SHIP undeflected and they are not efficiently registered by the TOF detectors. Therefore, after punching through the PSSD with an energy loss of a few MeV, they create a background in the region of the α particles from the decay of studied nuclei. By requiring an anticoincidence between the signals from this "veto" detector and from the PSSD detector,

a clear distinction between the decays and punch-through events can be made.

A large-volume four-fold segmented Clover germanium detector was installed behind the PSSD to measure the energies of γ rays detected within 5 μs of the detection of an EVR or α particle in the PSSD. The energy threshold for this detector was at $\sim$20 keV, which is above the energies of the possible L x rays of the Bi and At nuclei of interest. The absolute efficiency calibration for this detector is described in Ref. [25].

III. EXPERIMENTAL RESULTS

A. Identification of two isomeric states in ^{192}At

Figure 1(a) shows a part of the α spectrum registered in all 16 strips of the PSSD in anticoincidence with the signals from the TOF and "veto" detectors within time and position windows of 400 ms and 0.5 mm, respectively, after recoil implantation (events of the EVR-α1 type). The $E_{\alpha 1}$-E_γ spectrum of α1 events in coincidence with γ rays is given in Fig. 1(b), in which in addition to Tl and Bi K x rays a number of γ rays can be seen, e.g., at 36(1) keV, 117(1) keV, 149(1) keV and 165(1) keV. The α1(6995 keV)-γ(117 keV) and α1(7075 keV)-γ(149 keV) coincidence decays originate from ^{188}Bi [17] and ^{195}At [12], respectively; other decays will be discussed below. Figure 1(c) shows the same spectrum as in Fig. 1(a), but with an additional condition that the recoil-α1 pair must be followed by the α2 decay within time and position windows of $\Delta T(\alpha 1\text{-}\alpha 2) \leqslant 1$ s and $\Delta X(\alpha 1\text{-}\alpha 2) \leqslant 0.4$ mm, respectively (events of the EVR-[α1-α2] type). The strongly reduced intensity of the majority of activities in Fig. 1(c) in comparison with Fig. 1(a) is due to small α-branching ratios of respective daughter products and/or their longer half-life values in comparison with the time interval used in the α1-α2 correlation analysis. The two-dimensional $E_{\alpha 1}$-$E_{\alpha 2}$ spectrum corresponding to Fig. 1(c) is shown in Fig. 1(d). Due to the high intensity in Fig. 1(a) and relatively long search interval $\Delta T(\alpha 1\text{-}\alpha 2)$, some of the true recoil-α1 correlated decays (e.g., from ^{192}Po) occur in random correlations with α decays from other activities, which explains their presence in Figs. 1(c), (d). A few groups of correlated events with the energy $E_{\alpha 1} \geqslant 7180$ keV are present in Fig. 1(d) in the regions marked by the rectangles 'A,' 'B,' and 'C.'

An important comment on the α1-decay intensity in Figs. 1(c), (d) (EVR-[α1-α2] analysis) should be made here, which also applies to a number of spectra discussed below. Due to the $\sim$50% probability of α particles to escape from the PSSD in the backward direction, the α1-α2 correlation analysis reduces the number of true correlated α1 events in these spectra by a factor of two in comparison with Fig. 1(a) (EVR-α1 analysis). A similar loss of intensity also happens in the EVR-[α1-γ]-α2 analysis in comparison with the EVR-[α1-γ] analysis. However, the correlation with the known α decays of the daughter nuclei provides a unique identification of the parent isotopes, which in most cases outweighs the intensity reduction.

The measured half-life $T_{1/2} = 280(20)$ ms and energy $E_{\alpha 2} = 6815(10)$ keV for the α2 decays in region 'A' of Fig. 1(d) are in a good agreement with the decay properties of the $I^\pi = (10^-)$ α-decaying isomeric state in ^{188}Bi ($T_{1/2} = 265(10)$ ms, $E_\alpha = 6813(5)$ keV [17]; see also Fig. 7 of this paper). A weaker group in the rectangle 'C' at $E_{\alpha 2} = 7305(15)$ keV corresponds to the 7302(5) keV decay branch from the (10^-) isomer with an intensity of $I_{\alpha 2} = 3.6(10)\%$ relative to the 6813 keV decay [17].

Similarly, the measured half-life $T_{1/2} = 66(6)$ ms and energy $E_{\alpha 2} = 6995(10)$ keV for the strongest group of the α2 decays in the rectangle 'B' of Fig. 1(d) are in a good agreement with decay properties of the (3^+) isomeric state in ^{188}Bi ($T_{1/2} = 60(3)$ ms, $E_\alpha = 6992(5)$ keV [17] and Fig. 7 of this work). The assignment of the 6995 keV decay to this isomer is also confirmed by the observation of the α2(6995 keV)-γ(117 keV) coincidences expected for this decay, see Fig. 1(b) and Ref. [17]. As discussed in detail in Ref. [17], $\alpha + e^-$ summing in the PSSD of the energies of the α(6992 keV) decay and $\sim$30 keV prompt electrons resulting from the K-shell internal conversion of the 117 keV $E1$ transition leads to the higher-energy shoulder of the 6992 keV peak, which is also seen in our data. A weaker group at $E_{\alpha 2} = 7110(15)$ keV in the rectangle 'B' corresponds to the 7106(5) keV decay branch of the (3^+) isomer with an intensity of $I_{\alpha 2} = 2.1(2)\%$ relative to the 6992 keV line [17].

Based on the observed EVR-[α1-α2(^{188}Bi^{m1,m2})] correlations, the α1-events inside three regions 'A'-'C' of Fig. 1(d) are attributed to the decay of ^{192}At to two α-decaying isomeric states in the daughter ^{188}Bi nucleus. In this work we will follow the abbreviations of our study [17] in which the longer-lived $I^\pi = (10^-)$ and the shorter-lived $I^\pi = (3^+)$ α-decaying isomeric states in ^{188}Bi were denoted as ^{188}Bi^{m1} and ^{188}Bi^{m2}, respectively. For the sake of clarity we will not use the brackets for all I^π values in the following text, as all the spin and parity assignments mentioned in this work for ^{191,192,193}At and their respective daughters ^{187,188,189}Bi are tentative. However, all the tentative I^π values will be given in brackets in Fig. 7 and in Tables I and II.

One further comment on the quoted I^π assignments in ^{188}Bi should be made here. As stressed in Section 4.3 of Ref. [17], while the $I^\pi = 10^-$ assignment for ^{188}Bi^{m1} is well established by available experimental systematics, the 3^+ assignment for ^{188}Bi^{m2} is much less certain. This is because there is a clear deviation for ^{188}Bi^{m2} and its daughter ^{184}Tl^{m2} in comparison with the systematics of the low-spin states in the heavier odd-odd $^{190-196}$Bi and $^{186-192}$Tl isotopes (see Section 4.3.2 of Ref. [17] for details). Such a behavior may indicate a change in configuration of ^{188}Bi^{m2}, or in its daughter ^{184}Tl^{m2}, or in both of them. While the actual I^π assignment for ^{188}Bi^{m2} is not important for the identification of ^{192}At^{m2} in this section, it may be crucial for the construction of its decay scheme, see discussion in Sec. IV.

Figures 2(a) and 2(b) show the time distributions ΔT(EVR-[α1-α2]) between the recoil implantation and a pair of subsequent correlated α1-α2 decays for the events from the regions 'A' and 'B' of Fig. 1(d), respectively. The time distribution in Fig. 2(a) can be fitted with a single exponential function with the half-life value of $T_{1/2} = 88(6)$ ms, while Fig. 2(b) demonstrates two components with different half-lives. By using a simultaneous fit with two exponential functions shown by the dashed lines in Fig. 2(b), a good description of the

TABLE I. The measured decay properties of ^{192}At. Shown are isomer assignments, α-decay energies E_α, relative intensities I_α, reduced α widths δ^2_α, hindrance factors *HF* and energies and multipolarities of coincident γ rays. The γ-ray energy uncertainty is 1 keV. The reduced α widths were calculated with the Rasmussen prescription [11] by assuming $\Delta L = 0$ decays. The *HF* values were calculated relative to the average value of $\delta^2_\alpha = 58(7)$ keV for unhindered $7/2^- \rightarrow 7/2^-$ α decays in ^{191,193,195}At [12,13].

Isomer, I^π $T_{1/2}$ [ms]	E_α [keV]	I_α [%]	δ^2_α [keV]	*HF*	Coincident γ's [keV]
^{192}At^{m1}, $(9,10)^-$	7195(15)	4.0(7)	1.7(4)	34(9)	Bi *K* x rays, 165 *M*1, 188
88(6) ms	7224(15)	82(3)	28(4)	2.1(4)	64, Bi *K* x rays, 165 *M*1
	7385(15)	14(2)	1.4(3)	41(9)	
	7510–7560	$\leqslant$1.0(5)	$\leqslant$0.032(16)	$\geqslant$1800(900)	
^{192}At^{m2},	7363(15)	12(2)	11(2)	5.3(10)	Bi *K* x rays, 36 *E*1
11.5(6) ms	7435(15)	56(4)	30(4)	1.9(3)	36 *E*1
	7470(15)	31(3)	13(2)	4.5(8)	
	7510–7560	$\leqslant$1.0(5)	$\leqslant$0.25(13)	$\geqslant$230(115)	

full decay curve could be obtained with the half-life values of $T_{1/2} = 11.5(6)$ ms and $T_{1/2} = 85(10)$ ms for the shorter-lived and longer-lived components, respectively. The values of 85(10) ms from Fig. 2(b) and that of 88(6) ms from Fig. 2(a) can be considered as equal within the experimental uncertainty. This suggests that both components originate from the same isomer in ^{192}At which decays to *both* ^{188}Bi^{m1} (see Sec. III B) and to ^{188}Bi^{m2} (see Sec. III D). The ratio of the intensity of the 88 ms component in Fig. 2(a) to that in Fig. 2(b) is 1.6(1).

Thus, two different half-life values for decays attributed to ^{192}At identify two α-decaying isomeric states in this nucleus. The 88(6) ms isomer decaying to both ^{188}Bi^{m1,m2} will further be denoted as ^{192}At^{m1} (events in 'A' and the 85(10) ms component in 'B' of Fig. 1(d)), while the 11.5(6) ms isomer decaying to ^{188}Bi^{m2} will be denoted as ^{192}At^{m2} (the shorter-lived component from 'B' of Fig. 1(d)).

The $\alpha 1$ and $\alpha 1$-γ energy spectra for events from the regions 'A' and 'B' of Fig. 1(d) were used to establish the decay paths of ^{192}At^{m1,m2}. Figures 3(a)–(c) show the $\alpha 1$ and $\alpha 1$-γ energy spectra of the ^{192}At$^{m1} \rightarrow$ ^{188}Bi^{m1} decays from the region 'A,' while Figs. 4(a)–(c) and Figs. 5(a)–(c) provide the corresponding spectra from the region 'B' with

TABLE II. Main configurations and I^π assignments expected and observed in ^{192}At and in ^{188}Bi. The configurations based on the $\pi 3s_{1/2}$, $\pi 2f_{7/2}$, and $\pi 1i_{13/2}$ protons are the same in both nuclei. The deduced I^π assignments in column 3 are tentative and based on systematics and α-decay data, such as *HF* values and decay characteristics.

Configuration	Possible I^π	Observed I^π
$\pi 3s_{1/2} \times \nu 3p_{3/2}$	1^-, 2^-	
$\pi 3s_{1/2} \times \nu 1i_{13/2}$	6^+, 7^+	
$\pi 2f_{7/2} \times \nu 3p_{3/2}$	$2^+ \rightarrow 5^+$	
$\pi 2f_{7/2} \times \nu 1i_{13/2}$	$3^- \rightarrow 10^-$	$(9^-, 10^-)$[a]
$\pi 1i_{13/2} \times \nu 3p_{3/2}$	$5^- \rightarrow 8^-$	
$\pi 1i_{13/2} \times \nu 1i_{13/2}$	$0^+ \rightarrow 13^+$	
$\pi 1h_{9/2} \times \nu 3p_{3/2}$	$3^+ \rightarrow 6^+$	(3^+)[b]
$\pi 1h_{9/2} \times \nu 1i_{13/2}$	$2^- \rightarrow 11^-$	(10^-)[b]

[a]Only one state from this multiplet was observed in ^{192}At^{m1} and in ^{188}Bi^{m1} (at 165 keV); based on the available data both assignments are possible, see text.
[b]Observed in ^{188}Bi.

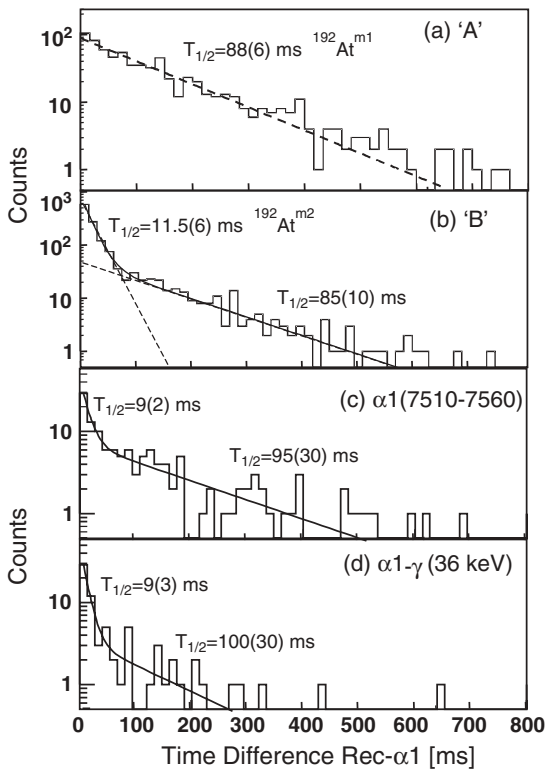

FIG. 2. Time distributions ΔT(EVR-$\alpha 1$) between the recoil and subsequent correlated α_1 decays. (a) and (b) Events from the EVR-[$\alpha 1$-$\alpha 2$] analysis for the regions 'A' and 'B' of Fig. 1(d), respectively. (c) and (d) Events from the EVR-$\alpha 1$ analysis: (c) Events with $E_{\alpha 1}$ = 7510–7560 keV from Fig. 1(a); (d) $\alpha 1$ events in coincidence with 36 keV γ ray from Fig. 1(b). The continuous lines in (b)–(d) show the result of the simultaneous fit by two exponential curves, see text for details. The dashed lines in panel (b) show the 11.5 ms and 85(10) ms components separately. The deduced half-lives and isotope assignments for different components are given.

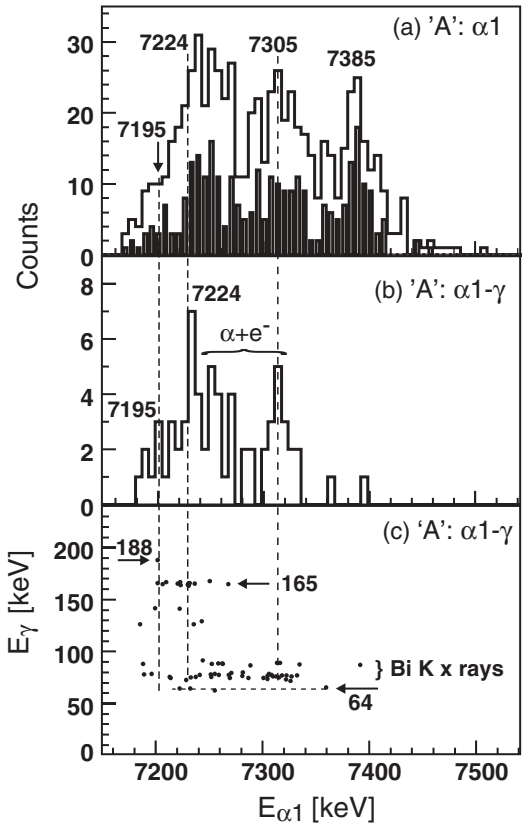

FIG. 3. (a) $\alpha 1$-energy spectrum for the $^{192}At^{m1} \rightarrow {}^{188}Bi^{m1}$ decays from the region 'A' of Fig. 1(d) with the conditions ΔT(EVR-$\alpha 1$) $\leqslant$ 400 ms and $\Delta T(\alpha 1\text{-}\alpha 2) \leqslant 1$ s. The open and solid histograms show the decays measured in all 16 strips or in eight strips with the best energy resolution, respectively. (b) The same spectrum as in (a) but requiring a coincidence with the γ decay of $E_\gamma \leqslant 250$ keV. (c) The two-dimensional $E_{\alpha 1}$-E_γ spectrum corresponding to (b). The α- and γ-decay energies are given in keV.

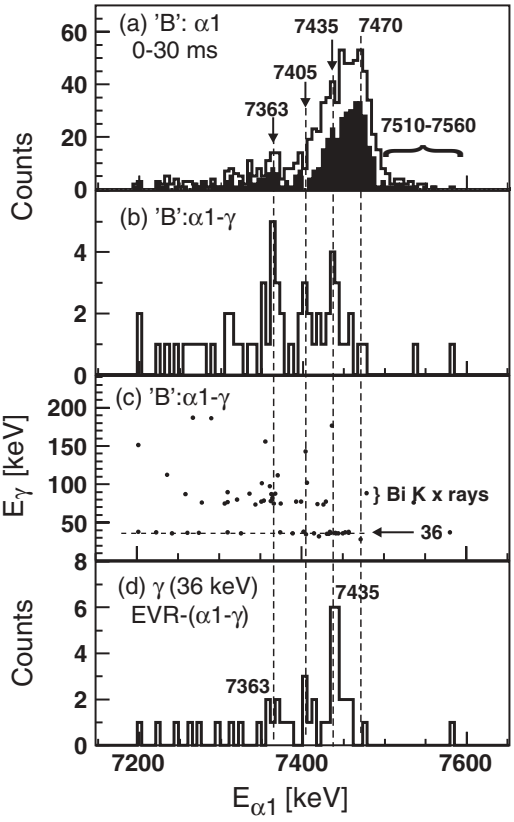

FIG. 4. (a) $\alpha 1$ decay spectrum for the events from the rectangle 'B' of Fig. 1(d) with the conditions ΔT(EVR-$\alpha 1$) $\leqslant$ 30 ms and $\Delta T(\alpha 1\text{-}\alpha 2) \leqslant 240$ ms. The open and solid histograms show the decays measured in all 16 strips or in eight strips with the best energy resolution, respectively. (b) The same spectrum as in (a) for the full PSSD, but in coincidence with γ decays of $E_\gamma \leqslant 250$ keV; (c) The two-dimensional $\alpha 1$-γ spectrum corresponding to (b). (d) $\alpha 1$ decays in coincidence with the 36 keV γ rays from the region marked by the rectangle in Fig. 1(b) (EVR-[$\alpha 1$-γ] analysis).

conditions ΔT(EVR-$\alpha 1$) $\leqslant$ 30 ms and ΔT(EVR-$\alpha 1$) = 70–400 ms, respectively. The latter conditions were chosen with the aim to highlight the $^{192}At^{m2} \rightarrow {}^{188}Bi^{m2}$ and $^{192}At^{m1} \rightarrow {}^{188}Bi^{m2}$ decays, respectively, by minimizing the contribution of the $T_{1/2} = 11.5$ ms isomer to the $\alpha 1$ spectrum of the $T_{1/2} = 88$ ms isomer and vice versa, while keeping the number of counts in both spectra high enough for subsequent α-γ analysis (Fig. 6). To account for the 60 ms half-life of $^{188}Bi^{m2}$ a condition $\Delta T(\alpha 1\text{-}\alpha 2) \leqslant 240$ ms was also applied to produce Figs. 4(a) and 5(a).

With the aim to show the full γ-ray intensity following the decay of ^{192}At, Fig. 6(a) shows a part of the γ-ray spectrum in coincidence with the $E_{\alpha 1} \geqslant 7180$ keV decays from Figs. 1(b) (events of the type EVR-[$\alpha 1$-γ] above the $\alpha 1$ decay of ^{192}Po). In the spectrum, in addition to the Bi K x rays, a few γ lines are seen, e.g., at 27(1) keV (8 events), 36(1) keV (74 events), broad structure denoted as 64(3) keV (30 events), 101 keV (15 events), 165 keV (41 events) and 188(1) (nine events). No statistically significant γ lines were observed above $E_\gamma = 200$ keV. As will be discussed below, most of these γ transitions originate from the excited states in ^{188}Bi fed by fine-structure α decays of ^{192}At.

The production cross section of ^{192}At was estimated as $\sigma = 40(10)$ nb by using the calculated SHIP efficiency of 40% [20,21].

B. $^{192}At^{m1} \rightarrow {}^{188}Bi^{m1}$ decay

α peaks at 7224(15) keV, 7305(15) keV, 7385(15) keV and, possibly, at 7195(15) keV can be distinguished in Fig. 3(a). The broadening of the 7224 keV peak is due to the $\alpha + e^-$ summing in the PSSD as discussed below. It is important to note that the same peaks are also seen in the spectrum registered in the eight strips of the PSSD with the best energy resolution (solid histogram in Fig. 3(a)).

Figure 3(b) shows the $\alpha 1$ decays registered in coincidence with the $E_\gamma \leqslant 250$ keV γ rays, while the corresponding two-dimensional $E_{\alpha 1}$-E_γ spectrum and its projection on the E_γ axis are shown in Fig. 3(c) and Fig. 6(b), respectively. The $\alpha 1$(7224 keV)-γ(165 keV) coincidences in Fig. 3(c) identify the fine structure $E_\alpha = 7224$ keV decay of $^{192}At^{m1}$ and the $E^* = 165$ keV excited state in $^{188}Bi^{m1}$ (see Fig. 7). Based on the similar total Q_α values for the $\alpha 1$(7224 keV)-γ(165 keV)

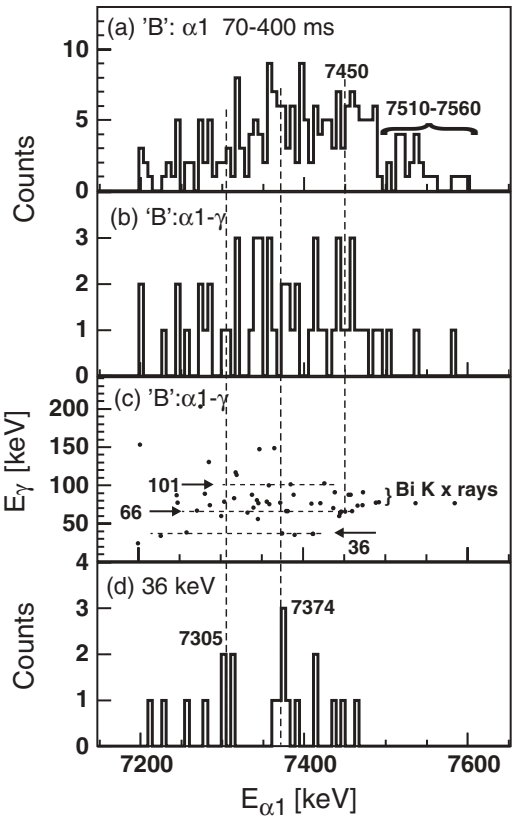

FIG. 5. (a) $\alpha 1$ decay spectrum for the events from the rectangle 'B' of Fig. 1(d) with the conditions ΔT(EVR-$\alpha 1$) = 70–400 ms and $\Delta T(\alpha 1\text{-}\alpha 2) \leqslant 240$ ms. (b) The same spectrum as in (a) but in coincidence with γ decays of $E_\gamma \leqslant 250$ keV; (c) The two-dimensional $\alpha 1$-γ spectrum corresponding to (b). (d) $\alpha 1$ decays in coincidence with the 36 keV γ rays from the EVR-[$\alpha 1$-γ] analysis. The α- and γ-decay energies are given in keV.

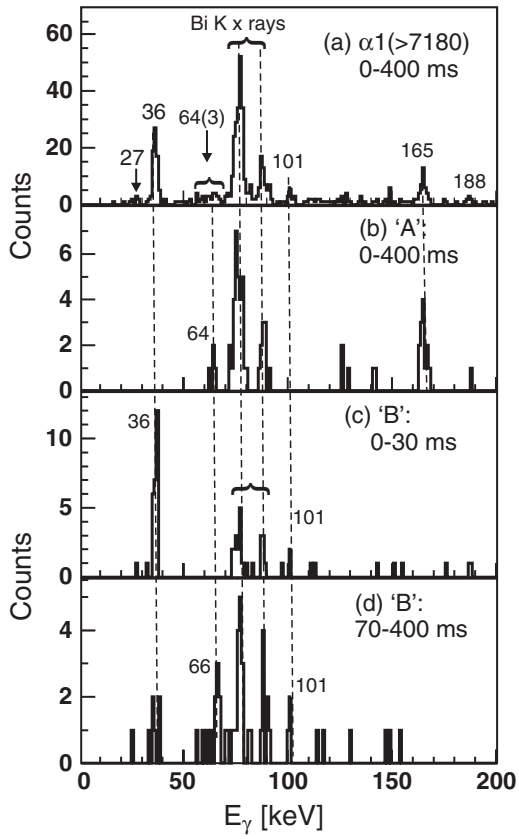

FIG. 6. Spectra of γ rays in coincidence with $\alpha 1$ decays ($\Delta T[\alpha 1\text{-}\gamma] \leqslant 5$ μs). (a) All $E_{\alpha 1} \geqslant 7180$ keV decays from Figs. 1(a), (b) (events of the type EVR-[$\alpha 1$-γ], ΔT[EVR-$\alpha 1$] $\leqslant 400$ ms). (b) $\alpha 1$ decays of $^{192}At^{m1}$ from the rectangle 'A' of Fig. 1(d) (events of the type EVR-[$\alpha 1$-γ]-$\alpha 2$, $\Delta T[\alpha 1\text{-}\alpha 2] \leqslant 1$ s); (c) $\alpha 1$ decays of $^{192}At^{m2}$ from the rectangle 'B' of Fig. 1(d) (ΔT[EVR-$\alpha 1$] $\leqslant 30$ ms), $\Delta T[\alpha 1\text{-}\alpha 2] \leqslant 240$ ms); (d) the same as (c) but for the ΔT[EVR-$\alpha 1$] = 70–400 ms time interval. The γ-ray energies are given in keV.

events and for the 7385(15) keV decay in Fig. 3(a), the latter decay is assigned as the full energy 'cross-over' transition to the 10^- state in $^{188}Bi^{m1}$, see Fig. 7.

The peak at 7305(15) keV in Figs. 3(a) and 3(b) is then understood as resulting from the full $\alpha + e^-$ summing in the PSSD of the energies of the 7224 keV decays and electrons of $E_{e,K} = E_\gamma(165\,\text{keV})\text{-}B_K(\text{Bi}) = 74.5$ keV originating from the K-shell internal conversion of the 165 keV transition, (B_K(Bi) = 90.5 keV is the Bi K-shell electron binding energy [22]). Partial summing with the electrons escaping from the PSSD explains the higher-energy tail of the 7224 keV decay denoted as '$\alpha + e^-$' in Fig. 3(b) and extending up to the full-energy summing peak at 7305(15) keV. This is also confirmed by the coincidences of the $\alpha + e^-$ events at $E_\alpha = 7230$–7320 keV with the Bi K x rays, see Fig. 3(c). Furthermore, the $\alpha + e^-$ summing with the L_{1-3}-shell electrons ($E_{e,L} \sim 150$ keV, as $B_{L_{1-3}}$(Bi) = 13.4–16.4 keV) will contribute, though with less intensity, to the energy region between the 7224 keV and 7385 keV peaks in Fig. 3(a). These inferences were confirmed by the GEANT Monte-Carlo simulations with the dedicated code developed for the SHIP detection system [23]. The simulations included the summing effects with the electrons and x rays from the K- and L-shell internal conversion of the 165 keV transition and also implemented different energy resolution of the PSSD's strips as observed in the experiment. Note that as the energy threshold in the Clover detector was at ~20 keV, which is above the energy of the Bi L x rays, no α-L x rays events are seen in our spectra.

By comparing the numbers of the full-energy $\alpha 1$(7224 keV)-γ(165 keV) coincident events and $\alpha 1$(7230–7320 keV)-Bi K x rays events from Fig. 3(c) (after normalization with the corresponding γ-ray detection efficiencies) a K-conversion coefficient of $\alpha_K(165\,\text{keV}) = 3(1)$ was deduced. This establishes a *M1* multipolarity for the 165 keV γ ray, as the theoretical conversion coefficients are $\alpha_K(E1) = 0.1$, $\alpha_K(E2) = 0.25$, $\alpha_K(M1) = 2.1$, $\alpha_K(M2) = 9.77$ [26]).

The higher-energy tail of the peak at 7385 keV in the open histogram in Fig. 3(a) practically disappears in the spectrum corresponding to the eight strips with the best energy resolution (Fig. 3(a), solid histogram). Therefore, we assume that these events are due to the strips with the poorer energy resolution. This is in agreement with the GEANT simulations which indeed show the tail above the 7385 keV.

In contrast to this, the group at 7195(15) keV is present in both spectra in Fig. 3(a). Some of these decays are in

coincidence with 165 keV γ decays (three events) and Bi K x rays (Fig. 3(c)). Based on the Q_α analysis, this α decay establishes an excited state at 190(15) keV in ^{188}Bi^{m1} with one of the deexcitation paths to the long-lived 10^- state proceeding via a cascade of 165(1) keV *M1* and yet unobserved low-energy $E_\gamma = 25(15)$ keV transitions. A single coincident 7203(15) keV-188(1) keV event in Fig. 3(c) is tentatively considered as evidence for the direct γ decay from this state to the 10^- state, which would determine the excitation energy of this state as $E^* = 188(1)$ keV.

The 64 keV γ transition (four counts, Figs. 3(c) and 6(b)) was observed in coincidence with broadly distributed α decays at $E_\alpha \sim 7200$–7360 keV. As three of the four counts at 64 keV are in coincidence with the 7224 keV decay (Fig. 3(c)), we assume the existence of a cascade consisting of 64 keV and yet unobserved 101 keV transitions, which form the second deexcitation path from the state at 165 keV in ^{188}Bi^{m1} (not shown in Fig. 7). The order of the transitions cannot be established from our data. Both transitions will most probably be partially converted, resulting in a cascade of the electrons which will additionally contribute to the $\alpha + e^-$ summing in the region between 7224 keV and 7385 keV peaks in Fig. 3(a).

The tentative cross-over ^{192}At$^{m1} \rightarrow {}^{188}$Bi^{m2} decay at 7510–7560 keV will be discussed in Sec. III D, in which also the evidence for the strongly-converted decay(s) from the state at 165 keV to states resulting from the proton-neutron multiplets (denoted by the 'p-n' in Fig. 7) in ^{188}Bi is presented.

The data for ^{192}At^{m1} are summarized in Table I and will be discussed in Sec. IV.

C. ^{192}At$^{m2} \rightarrow {}^{188}$Bi^{m2} decay

To highlight the 11.5 ms decays of ^{192}At, Fig. 4(a) shows the α1-energy spectrum from the rectangle 'B' of Fig. 1(d) for the time intervals of ΔT(EVR-α1) $\leqslant$ 30 ms and $\Delta T(\alpha 1$-$\alpha 2) \leqslant 240$ ms. A weak peak at 7363(15) keV along with two broader structures at ~7410–7480 keV and 7510–7560 keV are seen in Fig. 4(a), thus they must be attributed to the decay of ^{192}At^{m2}.

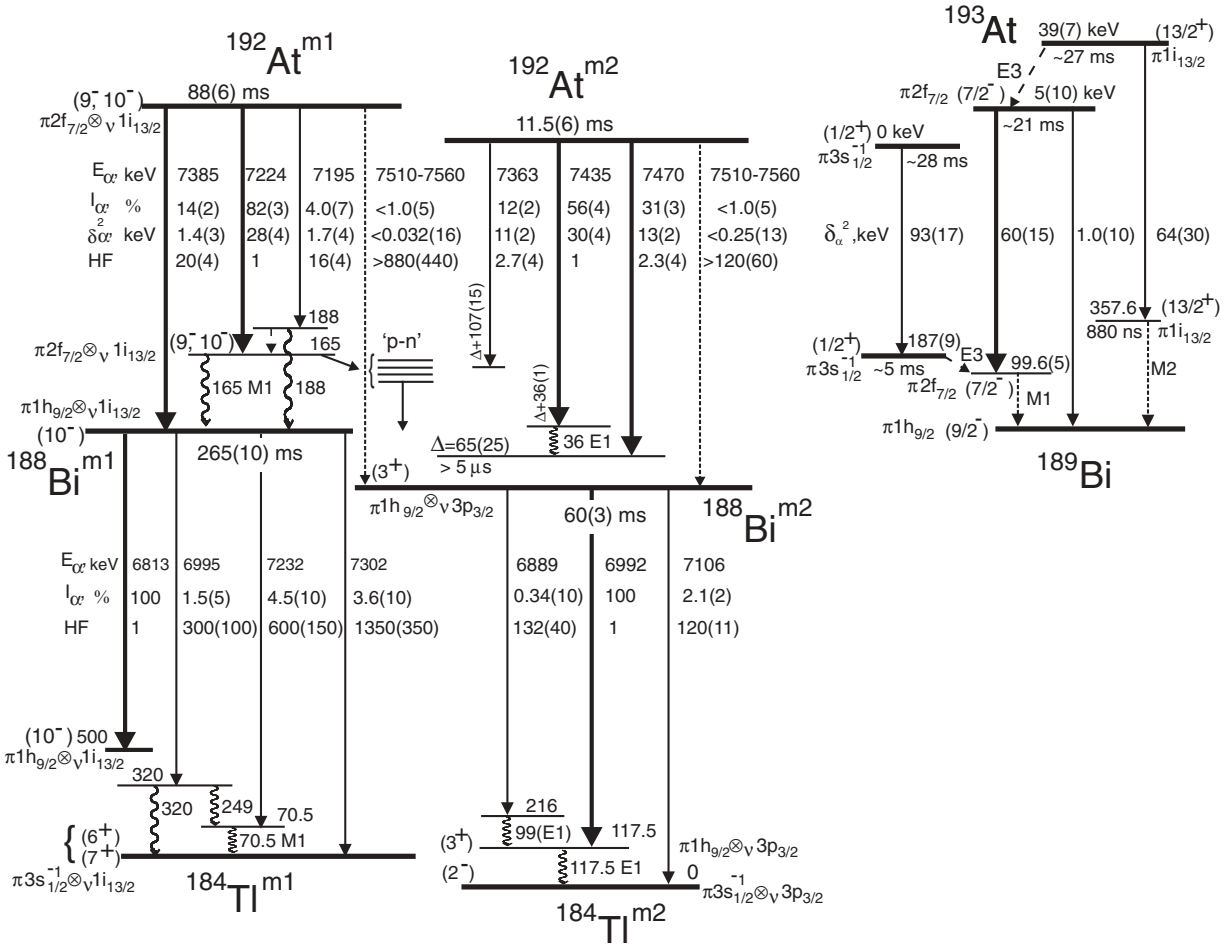

FIG. 7. Proposed decay schemes of ^{192}At^{m1,m2}. The decay schemes of the daughter isotopes ^{188}Bi^{m1,m2} were taken from Ref. [17]. The *HF* values are relative to the hindrance factor for the unhindered decay in each isomer, for which a normalized value of $HF = 1$ was adopted for this figure. The actual *HF* values relative to unhindered α decays in the neighbors ^{191,193,195}At are shown in Table I. The 7510–7560 keV decays, shown by the dashed lines, do exist in both isomers (see Table I), but their placement is uncertain (see text). The simplified partial decay scheme of ^{193}At was taken from Ref. [13]. All I^π assignments are tentative and based on the α decay pattern and systematics, see Refs. [13,17].

The $\alpha 1$ decays from Fig. 4(a) in coincidence with $E_\gamma \leqslant 250$ keV γ decays are shown in Fig. 4(b), while the corresponding two-dimensional $E_{\alpha 1}$-E_γ spectrum and its projection on the E_γ axis are given in Figs. 4(c) and 6(c), respectively. In addition to the 7363 keV peak, an α line at 7435(15) keV can be seen in Fig. 4(b). A weaker group at ~7405(20) keV results most probably from the $\alpha + e^-$ summing as discussed below.

Figure 4(c) shows that the 7435 keV decay is in coincidence with a 36 keV γ decay, being the strongest γ transition following the α decay of ^{192}At^{m2} (Fig. 6(c)). The total value $Q_{\alpha,\text{total}} = Q_\alpha(7435\,\text{keV}) + E_\gamma(36\,\text{keV})$ is equal within the experimental uncertainty to the Q_α value of the 7470 keV decay in Fig. 4(a). On this basis we assign the 7470(15) keV decay as the full-energy crossover transition to the state in ^{188}Bi^{m2} fed by the $\alpha(7435\,\text{keV}) + \gamma(36\,\text{keV})$ decays (see Fig. 7).

The 36 keV transition must be at least partially converted (e.g., $\alpha_{\text{tot,calc.}}(E1) = 1.5$, $\alpha_{\text{tot, calc.}}(M1) = 41$ [26]), resulting in conversion electrons with the energy of $E_e \sim 20$ keV (L-shell conversion) or $E_e \sim 33$ keV (M-shell conversion). The $\alpha(7435\,\text{keV}) + e^-(L,M)$ energy summing in the PSSD, along with the small summing with subsequent L- and M- x rays, broadens the 7435 keV peak toward the higher energy, up to the 7470 keV peak, which explains the broad structure at 7410–7480 keV in Fig. 4(a). Based on the observed number of the $\alpha 1(7435\,\text{keV})$-$\gamma(36\,\text{keV})$ coincident events in Fig. 4(c) (after normalization on the corresponding γ-ray efficiency), an *M1* or any higher multipolarity for the 36 keV transition must be ruled out, as otherwise the calculated intensity of the $\alpha + e^-$ summing peak alone would be by more than one order of magnitude stronger compared to the observed intensity of the *whole* 7410–7480 keV group. Therefore, an $E1$ multipolarity was assigned to the 36 keV transition.

It is important to note at this stage that the 36 keV transition also arises in the ^{192}At$^{m1} \rightarrow {}^{188}$Bi^{m2} decay branch (to be discussed in detail in the next section). This is confirmed by Fig. 2(d), which shows the time distribution between the recoil and subsequent pair of coincident $\alpha 1$-$\gamma(36\,\text{keV})$ events from the region denoted by the rectangle in Fig. 1(b). A shorter-lived $T_{1/2} = 9(3)$ ms and a longer-lived $T_{1/2} = 100(30)$ ms components are seen in Fig. 2(d), their half-lives being consistent within the experimental uncertainty with the half-life values of ^{192}At^{m2} and ^{192}At^{m1}, respectively.

The $\alpha 1$ spectrum in coincidence with the 36 keV γ rays from Fig. 1(b) is shown in Fig. 4(d) (EVR-[$\alpha 1$-$\gamma(36\,\text{keV})$] analysis). Figures 4(c), (d) prove that the 7363 keV decay is seen in coincidence with both Bi K x rays and 36 keV decays. This means that the 7363 keV decay feeds to an excited state in ^{188}Bi, which deexcites both by a partially converted $E_\gamma \geqslant B_K(\text{Bi}) = 90.5$ keV transition and by a cascade of transitions involving the 36 keV $E1\gamma$ decay. Based on the Q_α energy balance for the 7363(15) keV and 7470(15) keV decays, a still unobserved $E_\gamma = 107(15)$ keV decay could be a candidate for the former transition, which would define the energy of 71(15) keV for the γ ray being in cascade with the 36 keV transition. The K-shell conversion of the 107 keV decay would naturally explain the observed 7363 keV-Bi K x rays coincidences. Additionally, the $\alpha(7363\,\text{keV}) + e^-$ summing with the L- and M-shell conversion electrons from the coincident 36 keV $E1$ decay and yet unobserved 107 keV and 71 keV transition would then result in the higher-energy tail of the 7363 keV line extending nearly up to the 7470 keV decay.

The 36 keV transition is also seen in Figs. 4(c), (d) in coincidence with the extended region of α decays at 7200–7350 keV, which signifies the presence of other weaker yet unobserved fine-structure decays in ^{192}At^{m1,m2}, which feed to excited states whose de-excitation paths include the 36 keV $E1$ transition.

The highest-energy group at $E_{\alpha 1} = 7510$–7560 keV appears in Fig. 4(a) both for all 16 strips (open histogram) and for eight strips with the best energy resolution (solid histogram). The same structure is also seen in Figs. 1(a)–(d). The time distribution for these events, deduced from the recoil-$\alpha 1$ analysis (Fig. 2(c)), demonstrates two components with half-lives of $T_{1/2} = 9(2)$ ms and $T_{1/2} = 95(30)$ ms, which match within the experimental uncertainties the half-lives of ^{192}At^{m2} and of ^{192}At^{m1}, respectively (cf. also to Fig. 2(d)). From Fig. 2(c) we estimate that within a time interval of ΔT(EVR-$\alpha 1$) $\leqslant 30$ ms approximately two-thirds of the counts in the 7510–7560 keV group originate from ^{192}At^{m2} (11.5 ms decay), while the rest must be attributed to ^{192}At^{m1} (88 ms decay). Although we cannot separate the respective contributions within the given time interval due to the limited number of observed events, these data unambiguously prove that the highest-energy α decay of ^{192}At^{m2} has the energy in the range of 7510–7560 keV, see Fig. 7. From the intensity balance discussed above, an estimate of $I_\alpha(7510\text{–}7560\,\text{keV}) \leqslant 1.0(5)\%$ was deduced, see Table I.

Based on the energy difference between the 7470 keV α decay and the group at 7510–7560 keV, one has to assume that the former decay (and, therefore, the 7435 keV-36 keV pair) feeds an excited isomeric state at $\Delta = 65(25)$ keV in ^{188}Bi^{m2}, which deexcites by a long-lived $T_{1/2} >> 5$ μs transition, presumably to the 3^+ state in ^{188}Bi^{m2} (see Fig. 7). Otherwise, if the state at 65(25)keV were not isomeric, one would expect to observe the coincidences of the 7435 keV and 7470 keV decays with the γ ray(s) deexciting this state, which were not observed in our data. This nonobservation could be explained by the strong L- and M-shell conversion of the corresponding γ decay, but in this case the $\alpha + e^-$ summing peak at an energy $E_\alpha \sim 7480 + 65(25)$-$B(L,M) \sim 7530(25)$ keV would be expected with an intensity comparable to that of the whole broad peak at 7410–7480 keV. The latter inference follows from the GEANT simulations performed for this scenario. The nonobservation of such an intense structure in our data confirms the isomeric nature of the state at 65(25) keV in ^{188}Bi. It is worth noting that in the neighboring odd-mass ^{187,189}Bi isotopes long-lived isomeric states are known at an excitation energy below 200 keV (see Fig. 7 for ^{189}Bi.)

The deduced data and decay scheme of ^{192}At^{m2} are given in Table I and Fig. 7, respectively.

D. ^{192}At$^{m1} \rightarrow {}^{188}$Bi^{m2} decay

In this section we discuss the long-lived component in Fig. 2(b) which is presumably due to the ^{192}At$^{m1} \rightarrow {}^{188}$Bi^{m2} decay branch.

Figure 5(a) shows the spectrum of $\alpha 1$ decays from rectangle 'B' of Fig. 1(d) under conditions ΔT(EVR-$\alpha 1$ = 70–400 ms and $\Delta T(\alpha 1$-$\alpha 2) \leqslant 240$ ms. The events from Fig. 5(a) in coincidence with $E_\gamma \leqslant 250$ keV γ decays are shown in Fig. 5(b), while the corresponding two-dimensional $E_{\alpha 1}$-E_γ spectrum and its projection on the E_γ axis are given in Figs. 5(c) and 6(d), respectively.

The broad structureless $\alpha 1$ spectrum in Fig. 5(a) can only be explained by assuming that the parent α decay of ^{192}At is followed by a cascade of strongly converted low-energy γ transitions. The subsequent $\alpha + e^-$ summing in the PSSD then smears out the $\alpha 1$ decay spectrum for this component.

Based on the α-γ data in Figs. 5(b), (c) and 6(d) and anticipating the discussion of the proton-neutron multiplet states expected in the daughter ^{188}Bi, we propose the following scenario for the ^{192}At$^{m1} \rightarrow {}^{188}$Bi^{m2} decay (see Fig. 7). Namely, in addition to the 165 keV *M1* transition from the excited state at 165 keV decaying to the 10^- state in ^{188}Bi^{m1}, there should exist low-energy γ decays to a number of low-lying closely-spaced excited states decaying to ^{188}Bi^{m2}. As discussed in the next section, a multitude of such states is readily available from the coupling of the $\nu 1i_{13/2}$ and/or $\nu 3p_{3/2}$ neutrons to the low-lying $\pi 3s_{1/2}$, $\pi 1h_{9/2}$ and $\pi 1i_{13/2}$ proton orbitals (see Table II). Clearly, the decays from the 165 keV state to some of these states (schematically denoted by '*p*-*n*' in Fig. 7) and subsequent low-energy intramultiplet *M*1 and/or *E*2 γ transitions will be strongly converted, which results in the $\alpha + e^-$ summing in the PSSD. Two important observations confirm this scenario.

First of all, we note the strong presence of Bi *K* x rays (Fig. 6(d)) and a relatively low ratio of $I_\alpha/I_{\alpha\gamma} \sim 3.9$ of the number of α decays and α-γ decays in Figs. 5(a) and 5(b), respectively. For comparison, the corresponding ratios are $I_\alpha/I_{\alpha\gamma} \sim 10$ for the ^{192}At$^{m1} \rightarrow {}^{188}$Bi^{m1} decay (Figs. 3(a), (b)) and $I_\alpha/I_{\alpha\gamma} \sim 12.9$ for the ^{192}At$^{m2} \rightarrow {}^{188}$Bi^{m2} decay (Figs. 4(a), (b)). Thus, on average, each α decay from the ^{192}At$^{m1} \rightarrow {}^{188}$Bi^{m2} branch is accompanied by at least a factor of 2.5 more γ rays and/or Bi *K* x rays compared to the α decays from the ^{192}At$^{m1} \rightarrow {}^{188}$Bi^{m1} and ^{192}At$^{m2} \rightarrow {}^{188}$Bi^{m2} branches. Secondly, the spectrum in Fig. 5(a) starts at an energy of ~7220 keV, which corresponds to the energy of the strongest decay of ^{192}At^{m1} (E_α = 7224 keV), feeding to the 165 keV state. On these grounds we suggest the decay scheme for the ^{192}At$^{m1} \rightarrow {}^{188}$Bi^{m2} branch as shown in Fig. 7.

In addition to Bi *K* x rays, three peaks at 36(2) keV (five events), 66(1) keV (seven events) and 101(1) keV (three events) are seen in Fig. 6(d). All of them are in coincidence with the broadly-distributed $\alpha 1$ decays of ^{192}At^{m1} as shown in Fig. 5(c), thus the $\alpha + e^-$ summing is also important in these cases. Due to the low number of counts and broad energy distribution of the coincident α decays the placement of these γ rays was not possible.

We will only consider the 36(2) keV decay seen in coincidence with the broadly-distributed α decays at 7250–7410 keV in Fig. 5(c). This group cannot be due to the contribution from the 36 keV γ ray originating after decay of ^{192}At^{m2}. This is confirmed by the time distribution ΔT(EVR-[$\alpha 1$-γ(36 keV)]) events in Fig. 2(d), which shows the two components for the feeding coincident α decays. By using the exponential decay formula, a value of I_α(0–30 ms)/I_α(70–400 ms) ~ 67 can be estimated for the ratio of the number of decays in the 0–30 ms and 70–400 ms time intervals for the 11.5 ms α decay. Therefore, starting from 25 decays at 36 keV observed for the 11.5 ms component in Fig. 6(c) and by applying the above ratio, at most 0.37 counts at 36 keV can be expected in Fig. 6(d) due to the 11.5 ms component, while experimentally we observed five counts.

The spectrum of $\alpha 1$ decays in coincidence with the 36 keV transition from the EVR-[$\alpha 1$)-γ(36 keV)] analysis (ΔT(EVR-$\alpha 1$) = 70–400 ms) is shown in Fig. 5(d). The spectrum structure is clearly different compared to Fig. 4(d) which shows the corresponding analysis for ^{192}At^{m2}. Above data prove unambiguously that ^{192}At^{m1} feeds to an excited state in ^{188}Bi decaying further by the 36 keV transition, but no conclusion can be drawn on whether this state and the state fed by the 7435 keV of ^{192}At^{m2} are the same.

Finally, we discuss the group of 26 events at $E_{\alpha 1}$ = 7510–7560 keV in Fig. 5(a). Such a structure (14 counts) is also present in the spectrum, corresponding to the detectors with the best energy resolution (not shown for the sake of clarity of Fig. 5(a)). Presently this decay is tentatively shown in Fig. 7 as directly feeding to the 3^+ state in ^{188}Bi. However, two of these decays are in coincidence with the Bi *K* x rays (Figs. 5(c), (d)), which may indicate that this decay feeds to an excited state in ^{188}Bi which further decays by a partially *K*-shell converted transition to the 3^+ state. The resulting $\alpha + e^-$ summing would explain the broad energy distribution of this group.

In principle, a rough estimate of the relative position of two isomers in ^{192}At (and, therefore, in ^{188}Bi and ^{184}Tl) could be obtained based on observation of this transition. However, due to the placement and energy uncertainty discussed above we prefer not to deduce any definite values here.

IV. DISCUSSION

Spectroscopic studies of the odd-odd At and Bi isotopes are difficult due to a variety of closely-lying configurations expected in these nuclei. The recent α-decay studies of the odd-proton isotopes ^{191,193}At [13] are very helpful in this respect as they identified the lowest-lying proton states in the nuclei being the direct neighbors of ^{192}At studied in this work. As an example, the partial decay scheme of ^{193}At relevant for our discussion is shown on the right-hand side of Fig. 7. In ^{193}At three states ($1/2^+$, $7/2^-$ and $13/2^+$) were found within 39(7) keV of each other. In ^{191}At, no $13/2^+$ state has yet been observed, but the decay schemes of the known $1/2^+$ and $7/2^-$ states ($\Delta E^*(7/2^-$-$1/2^-) = 50(30)$ keV [13]) are qualitatively similar to that of the corresponding states in ^{193}At.

Therefore, in ^{192}At one expects the lowest configurations to be due to the coupling of the $\pi 3s_{1/2}$, $\pi 2f_{7/2}$ and, possibly, $\pi 1i_{13/2}$ protons to the $\nu 3p_{3/2}$ and/or $\nu 1i_{13/2}$ neutrons, which are known to be the lowest in the lead region in vicinity of the neutron midshell at $N = 104$. Table II summarizes the possible main configurations and I^π assignments expected in ^{192}At.

By analogy, the possible configurations in the daughter nucleus ^{188}Bi can be understood by considering the coupling of the valence $\nu 3p_{3/2}$ or $\nu 1i_{13/2}$ neutron to the lowest

proton-based states in the neighboring ^{187,189}Bi isotopes. In the latter nuclei, along with the $9/2^-$ ground state three excited states ($1/2^+$, $7/2^-$, $13/2^+$) were observed within 252 keV in ^{187}Bi or 358 keV in ^{189}Bi, see Fig. 7 for the latter case. Therefore, in ^{188}Bi one may expect a multitude (a few tens) of low-lying states in the range of 11^--0^-,0^+-13^+ within the energy interval of a few hundred keV which results from the *p-n* multiplets shown in Table II. Furthermore, multiple states with the same I^π originating from different multiples can be expected in ^{188}Bi, as for example three possible 8^- and three 3^+ states. Depending on their relative position, the states belonging to different *p-n* multiplets in ^{188}Bi may intermingle with each other, leading to a complex decay path between them. The previously known 10^- (^{188}Bi^{m1}) and 3^+ (^{188}Bi^{m2}) α-decaying isomeric states in ^{188}Bi have presumably the $\pi 1h_{9/2} \times \nu 1i_{13/2}$ and $\pi 1h_{9/2} \times \nu 3s_{1/2}$ configuration, respectively (Table II and Fig. 7), though, as mentioned in Sec. III A, the latter assignment is less certain.

α decay is a sensitive tool to study multiplet states in the odd-odd nuclei, as it selectively connects the states with the same spin, parity and configuration. For example, in our α-decay studies of the odd-odd $^{184-196}$Bi isotopes [15,17,18], the $\Delta L = 0$ $10^- \rightarrow 10^-$ and $3^+ \rightarrow 3^+$ α decays between the states of the same configuration and I^π values have been observed, unhindered when compared to their even-even neighbors. As an example, the $^{188}\text{Bi} \rightarrow {}^{184}$Tl decay can be seen in Fig. 7. In contrast, the spin-changing $\Delta L \neq 0$ α decays to other states of the *same* multiplet/configuration were strongly hindered, such as the $10^- \rightarrow 9^-$ decays in ^{194}Bi ($HF = 175(50)$) and in ^{192}Bi ($HF = 41(14)$). Even higher hindrance factors were deduced for the decays with a change of configuration and I^π values in these nuclei, see, for example the strongly hindered $10^- \rightarrow 6^+$ ($HF = 600(150)$) and $10^- \rightarrow 7^+$ ($HF = 1350(350)$) decays of ^{188}Bi^{m1} (Fig. 7) and extensive data for $^{184-196}$Bi isotopes in Refs. [15,17,18]. In terms of absolute intensity, practically all $\Delta L \neq 0$ α decays have intensities less than a few percent relative to the favored $\Delta L = 0$ decay. A similar pattern was also observed in the doubly odd $^{206,204,202}\text{Fr} \rightarrow {}^{202,200,198}\text{At} \rightarrow {}^{198,196,194}$Bi α-decay chains studied in Ref. [16].

Therefore, in the decay of ^{192}At^{m1,m2} a similar pattern can be expected with the strongest $\Delta L = 0$ unhindered α decay between the states of the same configuration and I^π along with much weaker $\Delta L \neq 0$ decays.

We start the discussion with the $^{192}\text{At}^{m1} \rightarrow {}^{188}\text{Bi}^{m1}$ branch. The hindrance factor for the 7224 keV α decay ($\delta^2_\alpha = 28(4)$ keV) in ^{192}At^{m1} relative to the unhindered $7/2^- \rightarrow 7/2^-\alpha$ decays in ^{191,193,195}At, all of them having a comparable reduced α width of $\delta^2_\alpha \sim 55$–60 keV [12,13], is $HF = 2.1(4)$, see Table I. The slight retardation of the 7224 keV decay is most probably due to a blocking effect, as seen, for example, in the comparison of the α decays of the odd- and even- mass Po nuclei [28]. Apart from this hindrance, the 7224 keV decay can be considered as a favored transition, which indicates that the configurations and I^π values of ^{192}At^{m1} and of the 165 keV state are the same. In contrast, the cross-over 7385 keV α decay is hindered by a factor of $HF = 20(4)$ relative to the 7224 keV decay (Fig. 7), thus the configurations and/or I^π values of ^{192}At^{m1} and of the 10^- α-decaying state in ^{188}Bi^{m1} must be different. A similar pattern is observed in ^{191,193,195}At, in which the full-energy crossover $7/2^- \rightarrow 9/2^-$ decays are hindered compared to unhindered $7/2^- \rightarrow 7/2^-$ decays [12,13], with the values of $HF = 47(6)$, 50(50) and 64(64) for ^{195}At, ^{193}At and ^{191}At, respectively (see Fig. 7 for ^{193}At).

Based on the assumed 10^- assignment for the α decaying state in ^{188}Bi^{m1} and an *M1* multipolarity for the 165 keV transition, a spin-parity of $I^\pi = 9^-$-11^- is plausible for the latter state. The $I^\pi = 11^-$ assignment can be ruled out, as otherwise the unhindered nature of the 7224 keV would establish the $I^\pi = 11^-$ value for ^{192}At^{m1}, which is not possible within configurations available for this nucleus in Table II. Therefore, only values of $I^\pi = 9^-$ or 10^-, both resulting from the $[\pi 2f_{7/2} \times \nu 1i_{13/2}]_{3^- - 10^-}$ multiplet, should be considered for the 165 keV state in ^{188}Bi^{m1} and for ^{192}At^{m1}. Since no unambiguous conclusion can be drawn in favor of either of them, we keep both possible assignments in Table II and Fig. 7. It is important to stress that the deduced configuration in ^{192}At^{m1} is based on the same proton $\pi 2f_{7/2}$ configuration as the $7/2^-$ isomers in the neighboring ^{191,193}At isotopes. This indirectly supports our inferences and confirms the expected onset of deformation in the At isotopes when approaching the neutron mid-shell at $N = 104$. Similarly, the $(9,10)^-$ 165 keV state in ^{188}Bi^{m1}, and the $7/2^-$ excited states at 63(10) keV in ^{187}Bi and at 99.6(5) keV in ^{189}Bi decaying by an *M1* transition are based on the same proton configuration.

The excited state at 188(1) keV in ^{188}Bi^{m1} fed by the 7195 keV hindered decay ($HF = 16(4)$) relative to the 7224 keV decay) could then be another member of the $[\pi 2f_{7/2} \times \nu 1i_{13/2}]_{3^- - 10^-}$ or $[\pi 1h_{9/2} \times \nu 1i_{13/2}]_{2^- - 11^-}$ multiplets.

In contrast to ^{192}At^{m1}, no configuration assignment can presently be made for the ^{192}At^{m2} isomer. There are a few reasons for this. First of all, as mentioned earlier, the configuration and $I^\pi = 3^+$ assignment for the daughter ^{188}Bi^{m2} isomer are less certain in comparison with those of the 10^- ^{188}Bi^{m1} isomer. Indeed, there is a clear deviation of the energy systematics for the presumable $3^+ \rightarrow 3^+$ and $3^+ \rightarrow 2^-$ decays of the low-spin isomer ^{188}Bi^{m2} in comparison with their trend in the heavier odd-odd $^{190-196}$Bi isotopes. Also, the 117 keV *E*1 transition in ^{184}Tl^{m2} does not follow the trend of the *E*1 decays in the heavier odd-odd Tl isotopes (see Fig. 8 of Ref. [17]). It is not clear if these effects are due to change of systematics in ^{188}Bi^{m2}, or in ^{184}Tl^{m2}, or in both of them. Therefore, in our analysis of the $^{192}\text{At}^{m2} \rightarrow {}^{188}\text{Bi}^{m2}$ branch we cannot rely on the properties of the daughter isotope as we could in the case of ^{192}At^{m1}. Furthermore, the multitude of the available closely-lying multiplet states in ^{188}Bi^{m2} results in many possible scenarios, most of which cannot be confirmed or discarded based on the available data. This is also reflected in a complex α spectrum of ^{192}At^{m2}: in addition to the 7435 keV and 7470 keV α decays, which have a comparable intensity, there are a few lower-intensity α lines, which are difficult to analyze in detail due to strong $\alpha + e^-$ summing effects.

An attempt was undertaken [29] to clarify the possible configurations by performing calculations of the energy splitting

within some of these multiplets, similar to those presented for the $[\pi 1h_{9/2} \otimes \nu 1i_{13/2}]_{2^-\rightarrow 11^-}$ multiplet in the odd-odd Tl and Bi nuclei in Ref. [27]. Unfortunately, it turned out that the results of the calculations are extremely sensitive to the parameters involving the $1i_{13/2}$ neutron shell. This is because both ^{192}At ($N = 107$) and ^{188}Bi ($N = 105$) are in vicinity of the $1i_{13/2}$ midshell at $N = 107$ where the proton-$\nu 1i_{13/2}$ coupling changes from the π(particle)-ν(particle) character to the π(particle)-ν(hole) character. This results in a strong degeneracy of the states within the multiplets for these configurations, which prevents us making any conclusions on their possible sequence. Therefore, we do not provide any configuration assignment for ^{192}At^{m2} based on the comparison with theoretical calculations.

Due to the same reasons as mentioned above, no exact decay path could be established for the ^{192}At$^{m1} \rightarrow {}^{188}$Bi^{m2} branch. As shown in Sec. III D the $I^\pi = 9^-, 10^-$ state at 165 keV partially decays by low-energy strongly converted transitions to a multitude of the lower-lying states, which in turn decay directly or indirectly to the 3^+ α-decaying isomer. However, due to lack of γ-γ coincidences and complex α-decay spectrum corresponding to this component, no further conclusions can presently be drawn.

V. CONCLUSIONS

Two α-decaying isomeric states with half-lives of 88(6) ms and 11.5(6) ms were identified in the new isotope ^{192}At, both of them having complex decay paths to the excited states in the daughter nucleus ^{188}Bi. The latter is due to the expected complexity and multitude of the states, resulting from the *p-n* multiplets in the odd-odd nuclei.

The $T_{1/2} = 88(6)$ ms high-spin $I^\pi = 9^-, 10^-$ isomer in ^{192}At is well understood as mainly resulting from the $[\pi 2f_{7/2} \times \nu 1i_{13/2}]_{3^-\rightarrow 10^-}$ configuration, which confirms the expected onset of deformation in the At isotopes by approaching the neutron midshell at $N = 104$. No unambiguous conclusion on the configuration or I^π value can be drawn for the 11.5 ms isomer.

Crucial for the present study was the understanding of the α-e^- summing in the PSSD. A more detailed study with much higher statistics and dedicated low-energy germanium detectors and low-energy electron detectors is necessary to resolve the complex decay pattern of these very neutron-deficient odd-odd nuclei.

Calculations of the proton-neutron coupling which would include the effect of deformation are clearly needed to understand the structure of the lightest odd-odd At isotopes.

ACKNOWLEDGMENTS

The authors thank A. De Maesschalck and K. Heyde for theoretical calculations and discussion of the proton-neutron multiplets in the lightest At and Bi nuclei. We thank the UNILAC staff for providing the stable and high intensity ^{51}V beam. This work was supported by the Access to Large Scale Facility programme under the Training and Mobility of Researchers programme of the European Union within the contract HPRI-CT-1999-00001, by the EXOTAG contract HPRI-1999-CT-50017, by the FWO-Vlaanderen and by the Interuniversity Attraction Poles Programme - Belgian State - Federal Office for Scientific, Technical and Cultural Affairs (IAP grant P5/07) and UK EPSRC. A.N.A. and J.J.R. were partially supported by the NSERC of Canada.

[1] P. Möller, J. R. Nix, W. D. Myers, and W. J. Swiatecki, At. Data Nucl. Data Tables **59**, 185 (1995).
[2] R. Julin, K. Helariutta, and M. Muikku, J. Phys. G: Nucl. Part. Phys. **27**, R109 (2001).
[3] A. N. Andreyev *et al*., Phys. Rev. C **69**, 054308 (2004).
[4] K. Van de Vel *et al*., Phys. Rev. C **65**, 064301 (2002).
[5] K. Van de Vel *et al*., Phys. Rev. C **68**, 054311 (2003).
[6] P. Nieminen *et al*., Phys. Rev. C **69**, 064326 (2004).
[7] M. B. Smith *et al*., J. Phys. G: Nucl. Part. Phys. **26**, 787 (2000).
[8] M. B. Smith *et al*., Eur. Phys. J. A **5**, 43 (1999).
[9] W. Mçczyński *et al*., Eur. Phys. J. A **3**, 311 (1998).
[10] M. Lach *et al*., Eur. Phys. J. A **9**, 307 (2000).
[11] J. O. Rasmussen, Phys. Rev. **113**, 1593 (1959).
[12] H. Kettunen *et al*., Eur. Phys. J. A **16**, 457 (2003).
[13] H. Kettunen *et al*., Eur. Phys. J. A **17**, 537 (2003).
[14] M. Leino *et al*., Nucl. Instrum. Methods Phys. Res. B **99**, 653 (1995).
[15] P. Van Duppen *et al*., Nucl. Phys. **A529**, 268 (1991).
[16] M. Huyse, P. Decrock, P. Dendooven, G. Reusen, P. Van Duppen, and J. Wauters, Phys. Rev. C **46**, 1209 (1992).
[17] A. N. Andreyev *et al*., Eur. Phys. J. A **18**, 39 (2003).
[18] A. N. Andreyev *et al*., Eur. Phys. J. A **18**, 55 (2003).
[19] W. Reisdorf, Z. Phys. A **300**, 227 (1981); W. Reisdorf and M. Schädel, *ibid*. **343**, 47 (1992).
[20] G. Münzenberg *et al*., Nucl. Instrum. Methods **161**, 65 (1979).
[21] S. Hofmann *et al*., Z. Phys. A **291**, 53 (1979); S. Hofmann and G. Münzenberg, Rev. Mod. Phys. **72**, 733 (2000).
[22] R. B. Firestone, *Table of Isotopes*, 8th ed. (John Wiley and Sons, Inc., New York, 1996).
[23] A. N. Andreyev *et al*., Nucl. Instrum. Methods Phys. Res. A **533**, 409 (2004).
[24] S. Saro *et al*., Nucl. Instrum. Methods Phys. Res. A **381**, 520 (1996).
[25] F. P. Heßberger *et al*., Eur. Phys. J. **A22**, 417 (2004).
[26] The program to calculate conversion coefficients. The National Nuclear Data Center (NNDC), http://www.nndc.bnl.gov/nndc/physco/.
[27] J. Van Maldeghem and K. Heyde, Fizika **22**, 233 (1990).
[28] K. Van de Vel *et al*., Phys. Rev. C **65**, 064301 (2002).
[29] A. De Maesschalck and K. Heyde, private communication (2005).